International Journal of Pharmaceutics 602 (2021) 120552

Contents lists available at ScienceDirect

International Journal of Pharmaceutics

journal homepage: www.elsevier.com/locate/ijpharm

Sequential administration of sialic acid-modified liposomes as carriers for epirubicin and zoledronate elicit stronger antitumor effects with reduced toxicity

Dezhi Sui [a], Xueying Tang [a], Junqiang Ding [a], Yang Wang [b], Ying Qin [a], Ning Zhang [a], Xinrong Liu [a], Yihui Deng [a], Yanzhi Song [a,*]

[a] College of Pharmacy, Shenyang Pharmaceutical University, Wenhua Road, No. 103, Shenyang 110016, China
[b] General Hospital of Fushun Mining Bureau of Liaoning Health Industry Group, Fushun, Liaoning, China

ARTICLE INFO

Keywords:
EPI
ZOL
Liposomes
Sequential administration
Combined administration
Co-loaded administration

ABSTRACT

Combined administration of drugs can improve efficacy and reduce toxicity; therefore, this combination approach has become a routine method in cancer therapy. The main combination regimens are sequential, mixed (also termed "cocktail"), and co-loaded; however, other combinations, such as administration of synergistic drugs and the use of formulations with different mechanisms of action, may exert better therapeutic effects. Tumor-associated macrophages (TAMs) play functional roles throughout tumor progression and exhibit characteristic phenotypic plasticity. Sialic acid (SA)-modified epirubicin liposomes (S-E-L) and SA-modified zoledronate liposomes (S-Z-L) administered separately kill TAMs, reverse their phenotype, and achieve antitumor effects. In this study, we examined the effects of a two-treatment combination for drug delivery, using sequential, mixed, and co-loaded drug delivery. We found that therapeutic effects differed between administration methods: mixed administration of S-E-L and S-Z-L, co-loaded administration of SA-modified liposomes (S-ZE-C), and sequential administration of S-E-L injected 24 h after S-Z-L did not inhibit tumor growth; however, sequential administration of S-Z-L injected 24 h after S-E-L resulted in no tumor growth, no toxicity to noncancerous tissue, and no death of mice, and exhibited 25% tumor shedding. Thus, our results thus encourage the further development of combined therapies for nanomedicines based on the mechanisms investigated here.

1. Introduction

Administration of drug combinations in cancer therapy has gained importance as a strategy to overcome the limitations of single mechanisms of action of traditional chemotherapy drugs (Vinciguerra et al. 2019), and this approach produces better overall therapeutic effects (Wu et al. 2020, Liu et al. 2020). However, mixed drug administration (termed cocktail) frequently fails to achieve the "right dose, right time, and right place" concept which is also termed the "3R principle" (Chou 2010, Hu et al. 2016). Therefore, developing novel combined-administration methods has become an important research objective; however, current efforts are mainly focused on sequential and co-loaded administration methods (Yang et al. 2019, Aryal, Hu and Zhang 2011).

Sequential administration can be adjusted according to individualized therapeutic regimens and can result in enhanced effects by improving the timing and by optimizing the nanoparticle carrier and drug dosage (Benyettou et al. 2017, Ottewell et al. 2010). Furthermore, injection with nanoparticles in batches may decrease off-target injury and multidrug resistance and may prolong the survival of patients; thus, sequential administration of drug combinations is preferred in clinical practice (Weber et al. 2016, (EBCTCG) (2019)). Co-loaded nanoparticles have been frequently used in preclinical studies for combined administration methods (Sun et al. 2015). Drugs with synergistic effects can be encapsulated in nanoparticles through interactions between the drug and the carrier (Liu et al. 2020, Kopecka and Lusa, 2016, Wei et al. 2016a), which facilitates decrease in the frequency of administration, lowers carrier-induced immune stimulation, and elicits alterations to the physical and chemical properties of the drugs through drug-drug interactions, potentially achieving the "3A" standard, i.e., "accurate proportions, accurate timing, and accurate places" (Wu et al. 2020, Liu et al. 2020). On August 3, 2017, the U.S. Food and Drug Administration granted regulatory approval to the first liposome-encapsulated combination of daunorubicin and cytarabine (VYXEOS; Jazz Pharmaceuticals,

* Corresponding author.
E-mail address: songyanzhi@syphu.edu.cn (Y. Song).

https://doi.org/10.1016/j.ijpharm.2021.120552
Received 28 December 2020; Received in revised form 3 March 2021; Accepted 25 March 2021
Available online 31 March 2021

Abbreviations

Full name	Abbreviation
zoledronate	ZOL
epirubicin	EPI
Sialic acid	SA
Sialic acid-modified zoledronate liposomes	S-Z-L
Sialic acid-modified epirubicin liposomes	S-E-L
Sialic acid-modified zoledronate and epirubicin liposomes	S-ZE-L
Sequential administration of S-Z-L injected 24 h after S-E-L	S-EZ-S
Sequential administration of S-E-L injected 24 h after S-Z-L	S-ZE-S
Co-loaded administration of SA-modified liposomes	S-ZE-C
Mixed administration of SA-modified liposomes	S-ZE-M
Tumor-associated macrophages	TAM
SA-modified DIR and EPI liposomes	S-DE-L
SA-modified DIR and EPI liposomes	S-DZ-L
SA-modified DIR, ZOL, and EPI liposomes	S-DZE-L

Inc.) for treating adult patients recently diagnosed with therapy-related acute myeloid leukemia or acute myeloid leukemia with myelodysplasia-related changes, which are variants of acute myeloid leukemia with poor prognosis.

Recent research focused on tumor microenvironments (Rodell et al. 2018). Tumor-associated macrophages (TAMs) account for a large proportion of tumor tissues (50%) and are present throughout tumor initiation and progression; therefore, they have attracted increasing research interest (R.H.Müller 1993). At present, there are mainly two TAM phenotypes: M1-like TAMs (classically activated macrophages) and M2-like TAMs (which replace activated macrophages). M1-like TAMs show higher levels of antigen presentation and induced immune responses; however, M2-like TAMs promote tumor growth and immunosuppression in most tumors. Therefore, the therapeutic objectives for TAMs may be summarized using the following four categories: 1. recruitment of monocytes is inhibited in the tumor microenvironment; 2. differentiation of TAMs is hindered; 3. colonized TAMs are killed; and 4. the phenotype of M2-like TAMs is reversed. To exploit the substantial expression of sialic acid (SA) receptors on the surface of TAMs, we synthesized SA octadecylamine (SA-ODA) conjugates and prepared SA-modified epirubicin (EPI) liposomes (S-E-L) designed to kill TAMs and SA-modified zoledronate (ZOL) liposomes (S-Z-L) designed to reverse the TAM phenotype. These two characteristics result in improved overall results in tumor treatment (Zhennan She et al. 2014, Zheng et al. 2019, Zhang et al. 2014, Ma et al. 2013). We investigated two aspects: 1) as these drugs can affect tumors through different mechanisms, we tested whether combined delivery would result in synergistically increased treatment effects, and 2) we examined whether sequential treatment, co-loading, or cocktail administration would be the optimal mode of drug delivery (Xia et al. (2018), Ovais, Guo and Chen 2019, Tang et al. 2020, Giarra et al. 2018).

To explore the efficacy of various combined administration regimens of EPI and ZOL in early tumor treatment, the co-loaded administration group (S-ZE-C) of SA-modified co-loaded liposomes (S-ZE-L), mixed administration group (S-ZE-M) of S-Z-L and S-E-L, sequential administration group (S-ZE-S) of S-E-L 24 h after S-Z-L, and sequential administration group injection (S-EZ-S) of S-Z-L 24 h after S-E-L injection were evaluated. S-Z-L was prepared using the passive loading method, whereas S-E-L and S-ZE-L were prepared using the ammonia ion gradient loading method (Gilad Haran et al., 1993). Therapeutic effects of the combined administration regimens were comprehensively analyzed based on *in vitro* and *in vivo* experiments. Our findings indicated that treatment with S-EZ-S resulted in no tumor growth, no injuries of noncancerous tissue, and no death in mice. Moreover, a 25% tumor shedding was observed.

2. Materials and methods

2.1. Materials

The following reagents were used: EPI·HCl (Olympic Star Pharmaceutical, Shenzhen, China), ZOL (Nanjing Jingrui Jiuan Biological, Nanjing, China), hydrogenated soy phosphatidylcholine ([HSPC]; A.V. T. Pharmaceutical, Shanghai, China), 1,1′-dioctadecyl-3,3,3′,3′-tetramethylindotricarbocyanine iodide ([DIR]; Molecular Probes, Eugene, OR, USA), SA (Changxing Pharmaceutical, Huzhou, China), octadecylamine ([ODA]; China National Medicines, Shenyang, China), N-hydroxysuccinimide ([NHS]; China National Medicines), cholesterol ([CH]; China National Medicines), and N-(3-dimethylaminopropyl)-N-ethylcarbodiimide HCl ([EDC·HCl]; China National Medicines). All other chemicals used in this study were of analytical or HPLC grade.

2.2. Cells and animals

RAW264.7 mouse macrophages and S180 sarcoma cells were obtained from the Cell Bank of the Chinese Academy of Sciences, Shanghai, China. Cells were cultured in RPMI 1640 medium supplemented with 10% Gemini Foundation fetal bovine serum (Meilun Biotechnology, Dalian, China).

Male Kunming mice were obtained from the Experimental Animal Center of the Shenyang Pharmaceutical University, Shenyang, China. All animal experiments were conducted in adherence to the relevant laws and institutional guidelines for the care and use of research animals of the Shenyang Pharmaceutical University Animal Studies Committee. The tumor-bearing mouse model was established by injecting 1×10^6 S180 cells in the left armpit of Kunming mice.

2.3. Synthesis and characterization of SA-ODA

EDC·HCl and NHS were used to couple SA and ODA. SA (2.3 g) was dissolved in 20 mL DMF at 70 °C. After cooling the solution to 25 °C, 1.75 g NHS and 2.85 g EDC·HCl were added, and the mixture was placed in an ice-water bath for 1 h. ODA (0.7 g) and 2.1 mL of triethylamine (TEA) were added and the reaction was incubated for 12 h in a water bath maintained at 60 °C. The crude product was dialyzed using a 1-kDa dialysis bag to remove impurities and was then lyophilized to yield SA-ODA (Zhennan She et al. 2014). The structure of SA-ODA was confirmed based on ^{1}H NMR using a Bruker spectrometer (Bruker 600-MHz, Bruker, Billercia, MA, USA) and mass spectrometry (MS; Agilent 1100, Agilent, Santa Clara, CA, USA).

2.4. Molecular docking

Specific recognition of SA-ODA by the receptor Siglec-1 was determined using molecular docking. Briefly, Siglec-1 (PDB: 1URL) was downloaded from the Protein Data Bank (http://www.rcsb.org/). Using PyMOL 2.0 software, Arg97, Arg105, and Leu107 were selected for cavity positioning. The structure of SD-ODA was visualized using ChemDraw 19.0 and docked to the selected 1URL cavity in a semi-flexible fashion using AutoDock 1.5.6 (Wei, Shimizu and Kanai 2016b).

2.5. Preparation of SA-modified liposomes

Liposomes were produced using modified ethanol injection (Ovais et al. 2019, Zhennan She et al. 2014, Miquel Pons and Estelrich, 1993). The membrane materials for producing S-Z-L, S-E-L, and S-ZE-L are listed in Table 1. Membrane materials were dissolved in absolute ethanol and were homogenized. Ethanol was evaporated at 60 °C to produce a phospholipid membrane, after which, a hydrating medium

Table 1
Liposome formulations (S-Z-L: the hydrating medium contained 0.18 mol/mL ammonium sulfate, 0.04 mol/mL $NH_3{\cdot}H_2O$ and 0.02 mol/mL ZOL, pH = 4.9; S-E-L: the hydrating medium contains only 0.2 mol/mL ammonium sulfate, pH = 4.9; S-ZE-L: the hydrating medium contains 0.18 mol/mL ammonium sulfate, 0.04 mol/mL $NH_3{\cdot}H_2O$ and 0.02 mol/mL ZOL, pH = 4.9).

Experiment	Drug	Loading method	Drug/Lipid (*mg/mg*)	Liposome composition (*n/n/n*)
S-Z-L	ZOL	Passive loading	2:25	HSPC/CH/SA-ODA (55/45/5)
S-E-L	EPI	Active loading	1:18	HSPC/CH/SA-ODA (55/45/5)
S-ZE-L	ZOL、EPI	Both	2:25、1:18	HSPC/CH/SA-ODA (55/45/5)

(Table 1) was added. The reaction mixture was incubated for 20 min. An ultrasonic cell pulverizer (JY92-IIDN; Ningbo Scientz Biotechnology, Ningbo, China) was used to sonicate the hydrated phospholipid at 180 W for 2 min and at 360 W for 6 min. Liposomes were sterilized by passing through a 0.22-μm microporous membrane. The liposome suspension (100 μL) was added to a Sephadex G-150 column and centrifuged at 2,000 rpm for 4 min. Then, it was washed twice using 50 μL distilled water and centrifuged at 2,000 rpm for 4 min to produce SA-modified ZOL liposomes (S-Z-L) and SA-modified blank liposomes (Tang et al. 2020).

To synthesize S-E-L and S-ZE-L, blank liposomes (1 mL) and S-Z-L (1 mL) with an ammonium ion gradient were incubated separately with 2.5 mg/mL EPI for 20 min, and free EPI was subsequently removed using a Sephadex G-150 column (Gilad Haran et al., 1993). Fluorescently labeled S-Z-L, S-E-L, and S-ZE-L liposomes were prepared (Ding et al. 2019) for determining *in vitro* uptake and *in vivo* distribution. S-Z-L, S-E-L, and S-ZE-L (2 mL each) were incubated with 20 μL of an absolute ethanol solution of DIR (10 mg/mL) for 20 min to prepare SA (0.2 mg/mL)-modified DIR and EPI liposomes (S-DE-L), SA (0.2 mg/mL)-modified DIR and ZOL liposomes (S-DZ-L), and SA (0.2 mg/mL or 0.4 mg/mL)-modified DIR, ZOL, and EPI liposomes (S-DZE-L).

2.6. Liposome characterization

The particle size and zeta potential of the S-Z-L, S-E-L, and S-ZE-L were determined using a NICOMP 380 HPL submicron particle analyzer (Particle Sizing Systems, Santa Barbara, CA, USA), and morphology of S-Z-L, S-E-L, and S-ZE-L was determined using transmission electron microscopy (JEM-2100, JEOL, Tokyo, Japan). S-Z-L, S-E-L, and S-ZE-L were diluted 100-fold and 10 μL of the diluted solutions was placed on a 200-mesh copper net and negatively stained using 1% phosphotungstic acid for 1 min, after which it was observed using transmission electron microscopy.

Encapsulation efficiency (EE) of the liposomes was determined as follows: S-E-L, S-Z-L, and S-ZE-L (100 μL, each) with unbound drug compounds were added to a Sephadex G-150 column and washed twice using 50 μL distilled water to remove the unbound drug compounds (200 μL = 100 μL + 50 μL + 50 μL, each). For EPI measurement, 100 μL liposomes before column processing and 200 μL liposomes after column processing were pipetted and demulsified in a 10-mL volumetric flask at constant volume (90% isopropyl alcohol containing 1.0 M HCl). Absorbance was measured before (A_b) and after column (A_a) separation using a UV-1801 UV/VIS Spectrophotometer (Beijing Rayleigh Analytical Instruments, Beijing, China) at 480 nm (Ding et al. 2019). For ZOL measurements, liposomes were lysed in a 20% Triton solution in a 2-mL volumetric flask, and absorbances at A_b and at A_a were determined using high-performance liquid chromatography (HPLC; Infinity system, Agilent). The chromatographic conditions for HPLC were as follows: Diamond C18 column (5 μm; 250 × 4.6 mm; Dalian Elite Analysis Instruments, Liaoning, China); λ = 224 nm; the mobile phase was acetonitrile/phosphate buffer (6/100, v/v), 20 mM tetra-*n*-butylammonium bromide, and 8 mM sodium pyrophosphate tetrabasic; pH 6.8 (Tang et al. 2020). EE was calculated using the following equation:

$$EE\% = A_a/A_b \times 100\%$$

2.7. In vitro drug release from liposomes

The cumulative rate of drug release from liposomes was calculated from the dialysis data. S-E-L, S-ZE-L (4 mL, each), and EPI solutions ([E-S]; 4 mL; 1.25 mg/mL) were filled in separate 10-kDa dialysis bags and placed in 100 mL of release medium (V_o = 100 mL; 2 M ammonium chloride, 0.2 M histidine; pH = 6.5). Similarly, S-Z-L, S-ZE-L, and ZOL solutions ([Z-S]; 0.1 mg/mL; 4 mL, each) were each filled in 10-kDa dialysis bags and placed in 50 mL PBS at 37 °C and agitated at a constant speed. Aliquots were collected (V = 4 mL) and added to an equal volume of fresh release medium, and the drug concentrations (C_n) were quantified spectrophotometrically at 480 nm (Ding et al. 2019, Cui et al. 2007). ZOL was quantified using HPLC.

The cumulative release rate, R_n, was calculated using the following equation:

$$R_n = \left(C_n V_o + \sum_{n-1}^{n} C_{n-1} V \right) \Big/ M_t \times 100\%$$

where M_t is the total amount of the drug in the dialysis bag.

2.8. In vitro cytotoxicity of RAW264.7 and S180 cells

RAW264.7 cells (1×10^6 cells/well) were inoculated in the upper chamber of a 0.4-μm Transwell six-well plate (Corning, Shanghai, China), and S180 cells were placed in the lower chamber at a 1:1 ratio of RAW264.7 to S180 cells (Cao et al. 2016). After 48 h of co-culturing, RAW264.7 cells were induced into M2-like TAMs (Fig. 4A) and were incubated with antibodies against Siglec-1, CD206, and F4-80 to determine the proportions of M2-like TAMs.

To determine whether toxicity to S180 and polarized RAW264.7 cells differed between methods of combined administration, 1×10^5 S180 cells/well and 1×10^5 polarized RAW264.7 cells/well were added to a 96-well plate. Cells were incubated for 12 h, after which, 10 μL of S-E-L, S-Z-L, or S-ZE-L (final concentration of EPI: 0.1 mg/mL, 0.05 mg/mL, 0.01 mg/mL, 0.001 mg/mL, 0.0001 mg/mL and final concentration of ZOL: 0.008 mg/mL, 0.004 mg/mL, 0.0008 mg/mL, 0.00008 mg/mL, 0.000008 mg/mL) were added; S-Z-L and S-E-L were mixed at equal proportions and added to S-ZE-M. The medium was replaced by drug-free medium after 24 h, and S-E-L and S-Z-L were added only in the sequential treatment group (Fig. 3A); MTT (5 mg/mL) was added after 24 h. A Model 680 Microplate Reader (Bio-Rad, Hercules, CA, USA) was used to measure OD_{570} values. The inhibition rate was calculated using the following equation:

$$\begin{aligned} Inhibition\,Rate = 1 - (&OD\,value\,of\,preparation\,treatment \\ &- OD\,value\,of\,preparation\,zero\,treatment)/(OD\,value\,of\,controls \\ &- OD\,value\,of\,blanks) \end{aligned}$$

Combination indices (CI) were calculated using the following equation:

$$CI = [C_A]_{50}/[A]_{50} + [C_B]_{50}/[B]_{50},$$

where $[C_A]_{50}$ and $[C_B]_{50}$ represent the IC_{50} values of A and B in different combined administration methods, respectively, and the denominators represent the IC_{50} values of single drugs A and B. Lower CI values indicate better combined effects of the drugs, and CI ≥ 1 indicates that there are no synergistic effects (Chou 2010).

2.9. M2-like Tams liposome uptake and phenotype reversal in vitro

DIR was inserted in the phospholipid bilayer of liposomes to produce liposomes with ZOL for uptake (Ex/Em = 748/780; DIR had strong anti-interference and was easy to detect). Polarized RAW264.7 cells were seeded in a six-well plate and cultured at 37 °C and 5% CO_2 for 12 h. S-DE-L, S-DZ-L, and S-DZE-L (DIR: 0.2 mg/mL) were added, and the medium was exchanged after 2 h (S-DE-L and S-DZ-L were added only in the sequential treatment; Fig. 3A). After 2 h, the cells were fixed using 4% paraformaldehyde, and 4,6-diamidino-2-phenylindole (50 μg/mL) was added. Cells were incubated for 20 min in the dark and visualized using confocal laser scanning microscopy (Carl Zeiss, Jena, Germany). Fluorescence intensities of EPI and DIR were detected using flow cytometry (Beckman Coulter, Fullerton, CA, USA). Data were analyzed using FlowJo 7.6.1.

To determine changes in receptor expression and proportions of M2-like TAMs, polarized RAW264.7 cells were seeded into a six-well plate and left undisturbed for 12 h. Cells were then incubated with S-Z-L, S-E-L, or S-ZE-L for 24 h (Fig. 3A) and harvested. Cell density was adjusted to 1×10^6 cells/mL and the cell suspension (100 μL) was incubated with 2 μL of anti-mouse F4-80 and 2 μL of anti-mouse CD206 primary antibodies at 4 °C for 30 min, followed by flow cytometry. One hundred microliters of cell suspension was incubated with 8 μL of PI (Meilun Biotechnology) at 25 °C for 15 min. After adding 400 μL binding buffer, the samples were analyzed using flow cytometry.

2.10. .Compound distribution in tissue in vivo

To examine tissue distribution of DIR-modified S-DZ-L (0.2 mg/mL DIR), S-DE-L (0.2 mg/mL DIR), and S-DZE-L (0.4 mg/mL DIR) liposomes, 72 tumor-bearing mice were randomly assigned to six groups (n = 12, each). The following treatments were used: S-DZ-L injection (S-Z-L), S-DE-L injection (S-E-L), S-DZ-L followed by S-DE-L after 24 h (S-ZE-S), S-DE-L followed by S-DZ-L after 24 h (S-EZ-S), S-DZE-L injection (S-ZE-C), and a mixture of S-DZ-L and S-DE-L (S-ZE-M). The dosage of DIR was 0.8 mg/kg in the S-ZE-C, S-ZE-M, S-ZE-S, and S-EZ-S treatments, and 0.4 mg/kg in the S-Z-L and S-E-L treatments. Two mice in each group were sacrificed 2, 12, 24, 26, 36, and 48 h post-treatment, and fluorescence images were obtained using an FX Pro *In Vivo* Imaging System (Carestream Molecular Imaging, Woodbridge, CT, USA) (Eisenblatter et al. 2009). Tumors, hearts, livers, spleens, lungs, and kidneys were collected for fluorescence imaging, and DIR was quantified in the liver and tumor tissues.

2.11. Pharmacodynamics

The left forearms of 48 Kunming mice were inoculated with 200 μL of suspended S180 cells (5×10^6 cells/mL), and the mice were randomly assigned to one of the following six treatment groups (n = 8, each): controls (5% glucose), S-E-L treatment, treatment with S-Z-L followed by S-E-L after 24 h (S-ZE-S), treatment with S-E-L followed by S-Z-L after 24 h (S-EZ-S), S-ZE-L injection (S-ZE-C), and treatment with a mixture of S-Z-L and S-E-L (S-ZE-M). Each treatment was administered every three days (ZOL dosage was 0.2 mg/kg and that of EPI was 2.5 mg/kg). Survival, body weight, and tumor volume were recorded daily; tumor volume was calculated by measuring the long (a) and short (b) diameters of the tumor and using the equation

$$\text{tumor volume} = 0.5 \times a \times b^2$$ (Liu et al. 2018).

The survival index (SI) used to evaluate toxicity and therapeutic effect outcomes was calculated according to the following equation:

$$SI = sum\ of\ body\ weights / sum\ of\ tumor\ weights\ of\ surviving\ mice) \ / \ (n - n_s)$$

where n is the total number of mice per group and n_s is the number of tumor-shedding mice in each group. Weight loss, tumor growth, and death decrease the SI; therefore, lower SI indicate lower quality of life and less efficient tumor treatment.

2.12. Tissue section staining

To observe damage to noncancerous and tumor cells in mice, tissue sections were prepared and immunofluorescence was measured. The hearts, livers, lungs, kidneys, and tumors of mice were fixed using 4% paraformaldehyde and were embedded in paraffin blocks. Embedded specimens were randomly sliced into 5-μm sections using an ultra-thin microtome, and paraffin was removed by heating to 70 °C. The samples were stained using hematoxylin and eosin, TUNEL reagent (Roche, Basel, Switzerland), anti-mouse CD68, and anti-mouse CD206 (CD68 and CD206 are markers of TAMs and M2-like TAMs, respectively), and observed using an inverted microscope.

To determine the ratio of M1-like and M2-like TAMs in tumors, an enzyme-linked immunosorbent assay kit (Elabscience Biotechnology, Houston, TX, USA) was used to quantify nitric oxide synthase 2 (iNOS/NOS2) and IL-10 in tumors (P Allavena and Mantovani 2012).

2.13. Statistical analyses

Data were analyzed using a two-tailed Student's *t*-test using SPSS version 23 (IBM Corp., Armonk, NY, USA). GraphPad Prism version 6 software (GraphPad, San Diego, California USA) was used to calculate IC_{50} values and to generate plots. Image-pro Plus version 6.0 (Media Cybernetics, Rockville, MD, USA) was used to assess fluorescence intensity. Data are presented as means ± standard deviation and statistical significance is reported at $P < 0.05$.

3. Results

3.1. Molecular docking, synthesis, and characterization of SA-ODA

We first examined whether SA-ODA, a derivative of SA, retained the ability to target Siglec-1. AutoDock 1.5.6 software was used to simulate the interaction of SA-ODA with the Siglec-1 receptor. We observed that Arg97 and Arg105 in the Siglec-1 receptor interacted with SA-ODA interacted via hydrogen bonding (Fig. 1A). The binding energy value was − 0.72, the KI was 512.16 mM, and the unbound extended energy was − 5.82 (Table 2). As binding energy was < 0, SA-ODA can apparently spontaneously bind to Siglec-1.

3.2. Preparation and characterization of liposomes

Zeta potential, particle size, EE%, cumulative release rate, and morphology are important parameters for liposome characterization (Makwana et al. 2021). The zeta potentials of S-Z-L, S-E-L, and S-ZE-L ranged from − 10 to − 20 mV, particle sizes were 105–115 nm, encapsulation rate was approximately 5% for ZOL and over 95% for EPI (Table 3). The release rates of EPI and ZOL from liposomes differed significantly between EPI and ZOL drug solutions. The cumulative release rate of ZOL from S-Z-L was 1.5 × -fold higher than that of ZOL from S-ZE-L at 48 h (Fig. 2C). Occurrence of "coffee bean" particles with particle sizes of 100–120 nm in S-E-L and S-ZE-L is shown in Fig. 2B.

3.3. Cytotoxicity and uptake in polarized RAW264.7 cells in vitro

The extent and time of liposome uptake by cells differed between treatments and directly affected interactions between liposomes and cells. S-EZ-S and S-ZE-S showed that uptake of the first dose was the same as that in S-E-L and S-Z-L; however, a slight, albeit not statistically significant, decrease in the intake of liposomes of the second dose was

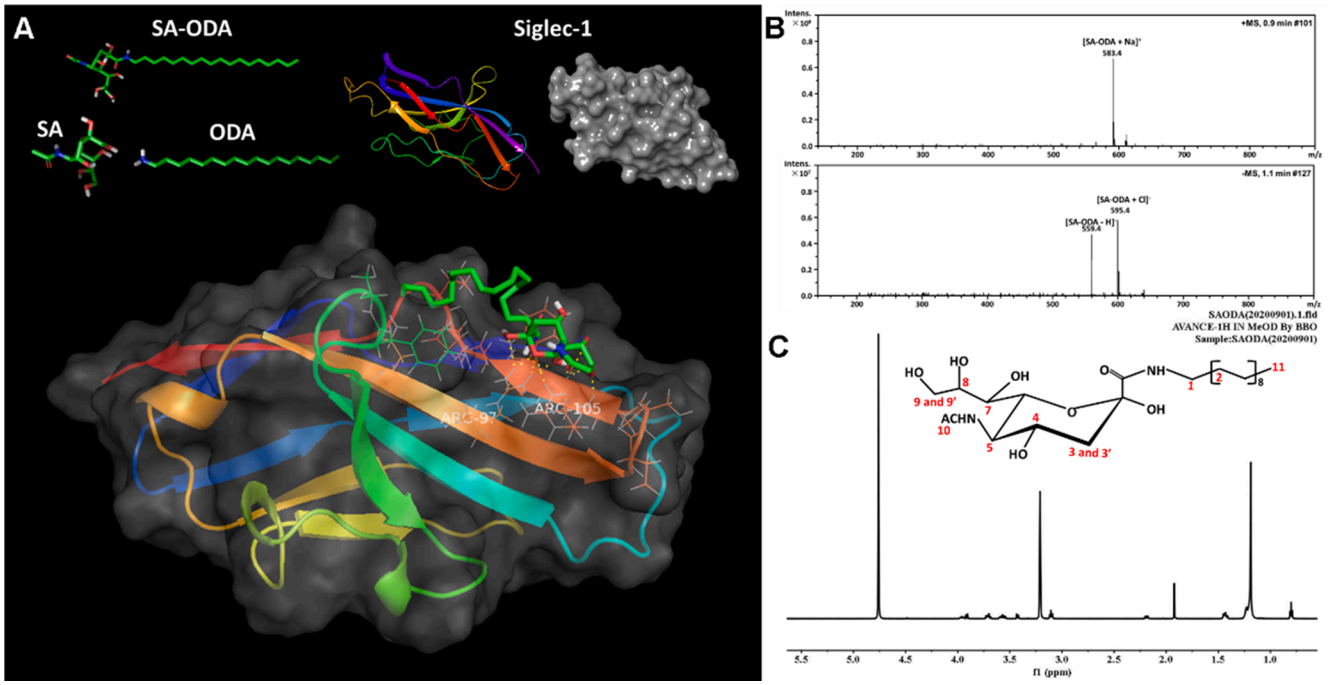

Fig. 1. Validation of receptor targeting by and characterization of SA-ODA. (A) Molecular docking of SA-ODA into the Siglec-1 SA-binding cavity (PDB: 1URL). (B) MS and (C) ^{1}H NMR spectrum of SA-ODA.

Table 2
Parameters and the docking site of Siglec-1 and SA-ODA.

Parameter	Value	Docking site
Binding Energy	−0.72	Siglec-1 SA-ODA
KI	296.58 mM	Siglec-1:A:ARG97:HH21:SAODA::1:O
Intermolecular Energy	−8.77	Siglec-1:A:ARG97:HH21:SAODA::1:O
Internal Energy	−5.82	Siglec-1:A:ARG97:HH21:SAODA::1:H
Torsional Energy	8.05	Siglec-1:A:ARG105:HN:SAODA::1:O
Unbound Extended Energy	−5.82	Siglec-1:A:ARG105:O:SAODA::1:H

Table 3
Characterization of liposomes (n = 3).

Liposome	Zeta potential (mV)	Partical size (nm)	PDI	EE (%)	DL (g/g)
ZOL liposome	−10.0 ± 1.98	106 ± 1.11	0.124 ± 0.011	5.86 ± 1.05	0.003 ± 0.001
EPI liposome	−12.0 ± 2.19	108 ± 1.02	0.111 ± 0.010	92.3 ± 1.23	0.030 ± 0.002
Co-loaded liposome	−11.0 ± 2.08	112 ± 0.89	0.122 ± 0.010	EPI:91.2 ± 1.23 ZOL:5.04 ± 1.34	0.032 ± 0.003

*DL (Drug loading) = EE(%)×(W_{durg} / $W_{lip+CH+SA-ODA}$).

observed (Fig. 3B and C). The overall uptake in the mixed administration treatment (S-ZE-M) was significantly lower than that in the other treatments (Fig. 3B and C). IC_{50} was significantly lower in S-EZ-S than in S-ZE-M (Table 4), and the CI was < 1. Apoptosis rates in cells of the S-EZ-S treatment were significantly higher than those in the other treatments with 0.025 mg/mL EPI and 0.002 mg/mL ZOL (concentrations of the drug in liposomes at the time of injection). These findings indicate that S-EZ-S treatments may elicit synergistic effects. In S180 and RAW264.7 cells, ZOL concentrations at the time of injection were lower than the IC_{50} value of ZOL in the S-Z-L treatment, and EPI concentrations at the time of injection were higher than the IC_{50} value of EPI in the S-E-L treatment with different combinations.

3.4. Phenotypic reversal of M2-like TAMs in vitro and in vivo

The concentration of ZOL in peripheral blood of mice was below the IC_{50} value of the S-Z-L treatment; thus, ZOL did not kill M2-like TAMs, rather reversed their phenotype in different combination treatments. The *in vitro* experiment showed that co-culturing S180 and RAW264.7 cells could induce polarization of over 90% of the RAW264.7 cells (Fig. 4A); however, cytotoxicity and phenotypic reversal effects on M2-like TAMs differed between the combination treatments (Fig. 4B and C). Fluorescence intensity of CD206 was significantly lower after the S-EZ-S treatment than after the S-ZE-S, S-ZE-C, and S-ZE-M treatments ($P < 0.001$), and fluorescence intensity of PI was significantly higher than that in the S-ZE-S, S-ZE-C, and S-ZE-M treatments ($P < 0.01$). *In vivo*, the S-EZ-S treatment showed lower fluorescence intensities of CD68 and CD206 and lower cell densities compared to the S-ZE-S, S-ZE-C, and S-ZE-M treatments (Fig. 5). After S-EZ-S treatment, IL-10 release by M2-like TAMs was significantly reduced ($P < 0.01$), whereas no significant effect on the release of iNOS/NOS2 was observed (Fig. 8D). Results from *in vitro* and *in vivo* experiments indicated higher TAMs killing and phenotypic reversal ability of S-EZ-S treatment compared to the other treatments.

3.5. Compound distribution in tissues in vivo

The use of DIR - liposomes facilitated monitoring liposome tissue distribution which demonstrated differences between combined administration methods (Fig. 6A and B). DIR accumulation in the liver from 0 to 48 h did not differ significantly between S-ZE-S and S-EZ-S treatments, and DIR fluorescence intensity was significantly higher than that in tumors after the S-ZE-C treatment for 48 h ($P < 0.001$). DIR accumulation achieved a maximum value in the co-loaded S-ZE-C and mixed S-ZE-M treatments, and DIR fluorescence intensity was significantly higher than that in the liver after the S-EZ-S treatment for 2 h ($P < 0.001$). DIR accumulation was significantly lower in tumors after 24 h and after the S-ZE-C treatment, compared to the S-EZ-S treatment ($P < 0.05$; Fig. 6B). However, only small amounts of DIR had accumulated in the heart, spleen, lung, and kidneys from 0 to 48 h in all combined administration treatments.

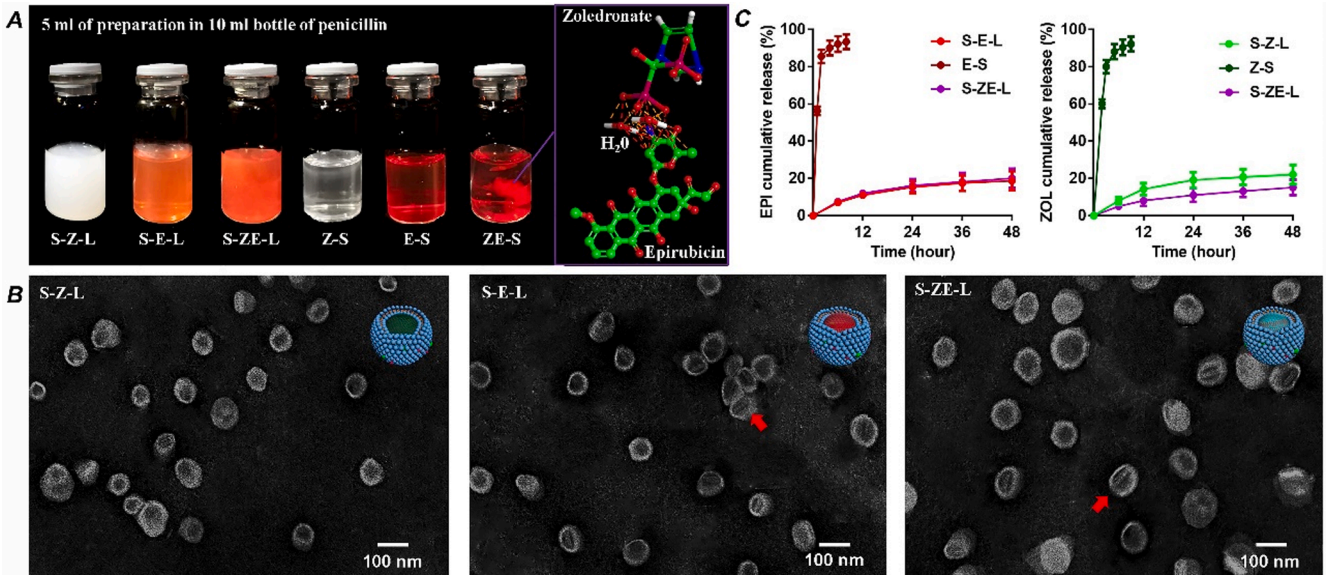

Fig. 2. Liposome characterization. (A) Liposome appearance ZOL solutions (Z-S), EPI solutions (E-S), and mixed solutions of EPI and ZOL (ZE-S). Simulation of interactions between ZOL and EPI in the S-ZE-L (ZE-S). (B) Transmission electron micrographs of the liposomes (Scale bar: 100 nm, the red arrows mark the low-solubility aggregates). (C) *In vitro* drug release from E-S and Z-S liposomes (n = 3).

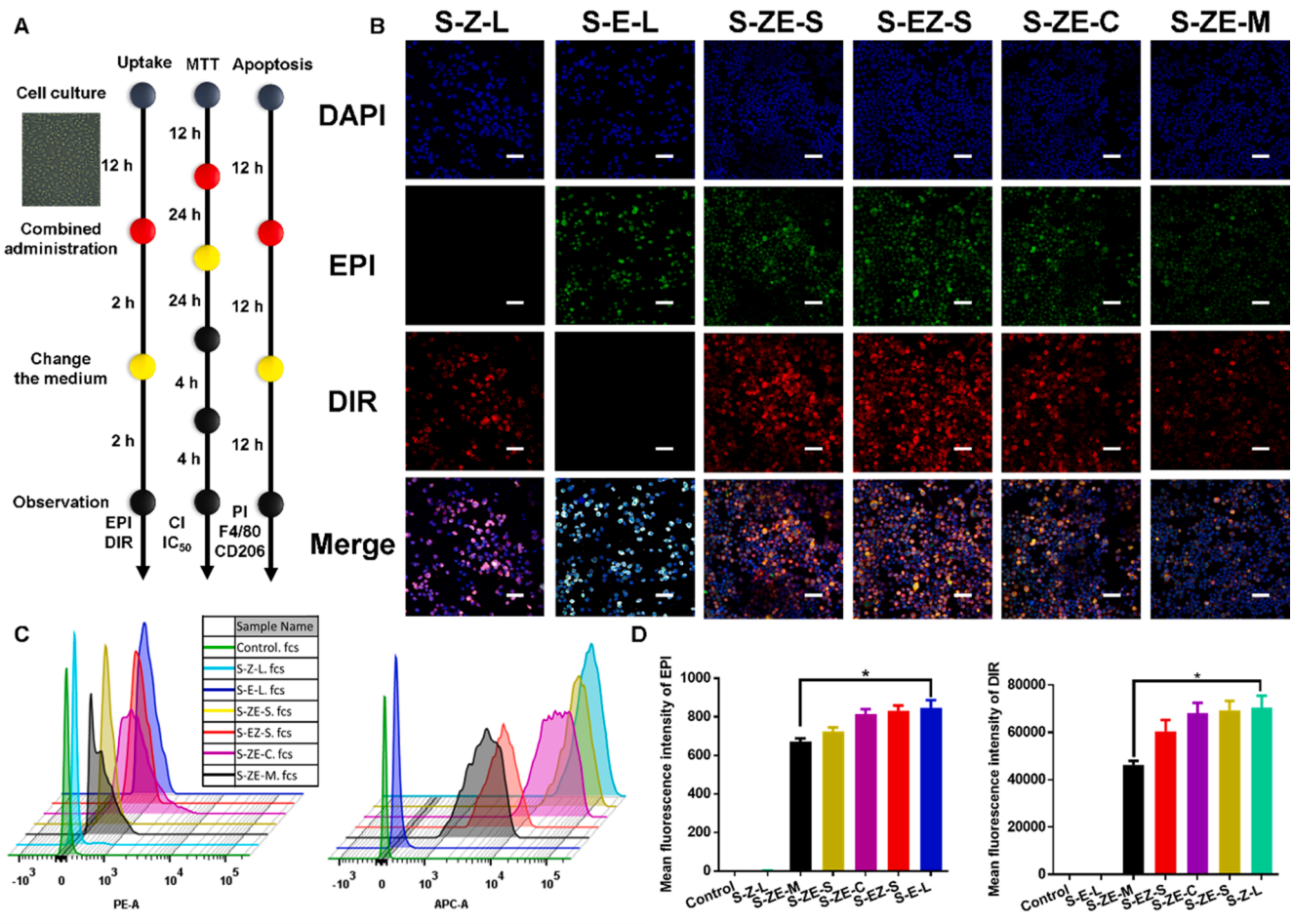

Fig. 3. Uptake in polarized RAW264.7 cells of liposomes administered by different combination methods. (A) Experimental procedures for MTT, cellular uptake, and apoptosis assays. (B) The cellular uptake of liposomes observed by confocal microscopy (Green fluorescence is EPI, red fluorescence is DIR. Scale bar = 100 μm.) and analyzed by the flow cytometry (C, D) DAPI staining (blue) indicates cell nuclei ($P^* < 0.05$).

Table 4
IC_{50} values and Combination Indices (CI) of different combined administration methods (n = 3).

Cells	Parameter	S-Z-L	S-E-L	S-ZE-S	S-EZ-S	S-ZE-C	S-EZ-M
S180 Cells	IC_{50} (×100 mg/L)	0.181 ± 0.015	0.158 ± 0.012	0.156 ± 0.011	0.157 ± 0.009	0.159 ± 0.011	0.175 ± 0.014
	CI	–	–	0.978 ± 0.11	0.988 ± 0.10	1.00 ± 0.09	1.10 ± 0.08
	Inhibition Rate of 0.025 mg/mL EPI and 0.002 mg/mL ZOL			72.2%±0.01	85.1%±0.03	63.2%±0.01	60.2%±0.02
RAW264.7 Cells	IC_{50} (×100 mg/L)	0.1087 ± 0.007	0.171 ± 0.018	0.162 ± 0.014	0.150 ± 0.012	0.164 ± 0.017	0.174 ± 0.020
	CI	–	–	0.989 ± 0.09	0.916 ± 0.06	0.999 ± 0.07	1.06 ± 0.10
	Inhibition Rate of 0.025 mg/mL EPI and 0.002 mg/mL ZOL			58.2%±0.02	71.2%±0.02	60.1%±0.03	55.4%±0.03

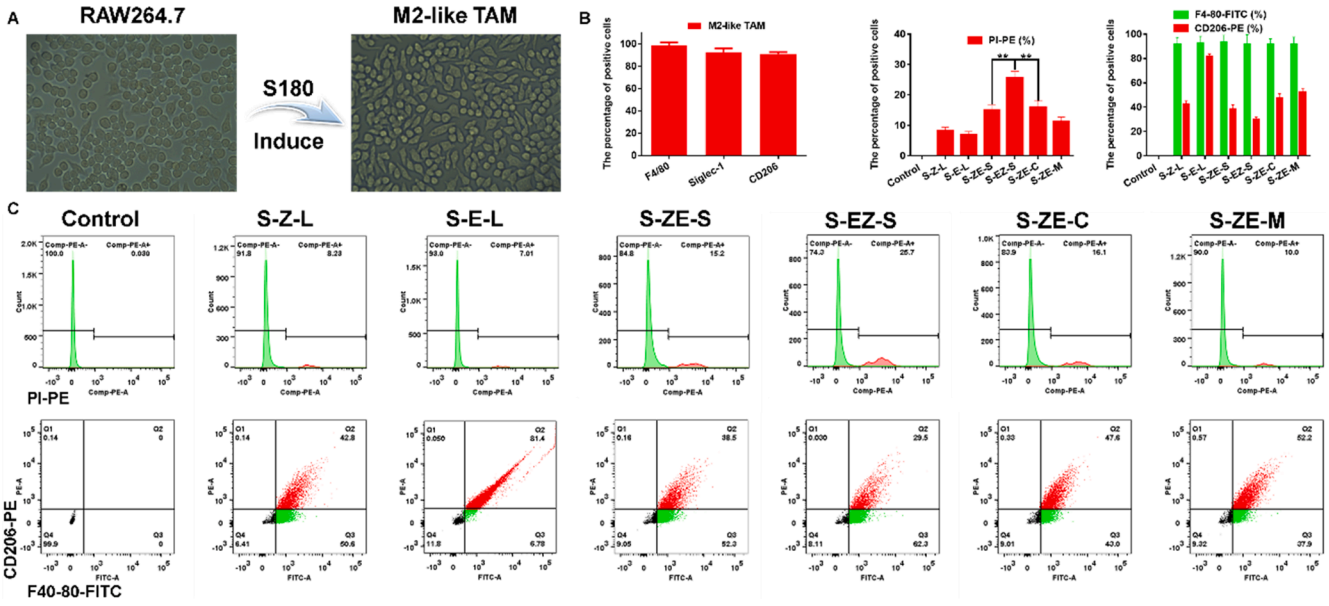

Fig. 4. The reverse of TAMs phenotype *in vitro*. (A) Expressions of F4/80 , CD206, and Siglec-1 receptors on the surface of M2-like TAMs (n = 3). (B, C) Expression of PI-PE, CD206-PE, and F4/80-FITC on the surface of M2-like TAMs after incubation with liposomes (n = 3) (P** < 0.01).

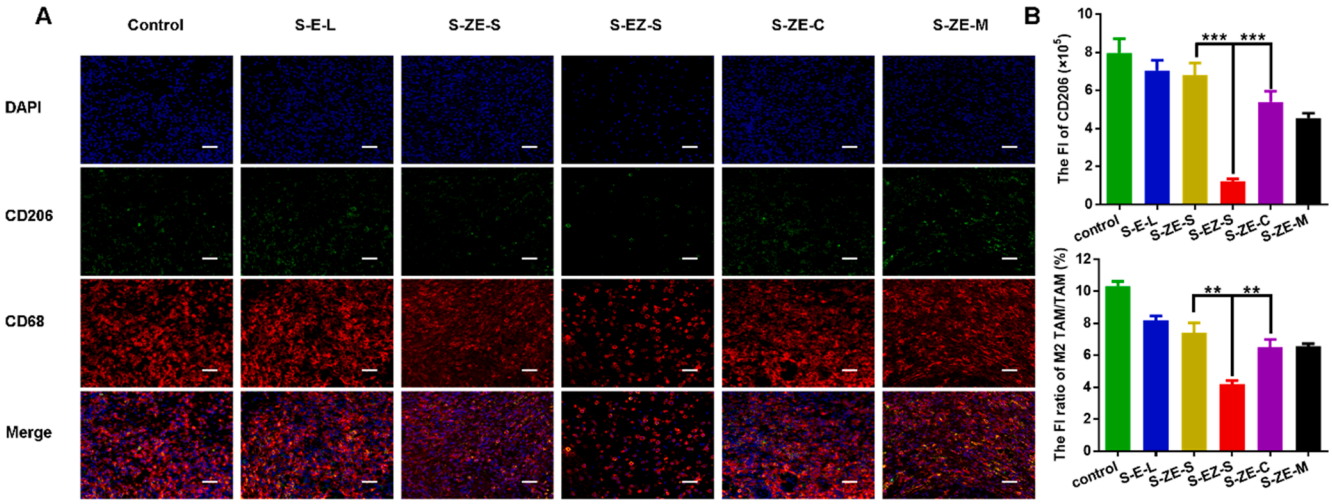

Fig. 5. (A) Immunofluorescent staining of the tumor tissue for CD206 (green) and CD68 (red), expressing CD206 and CD68 typical TAMs markers. Scale bar = 50 μm. (B) Analysis of immunofluorescent staining fluorescence intensity (The fluorescence intensity ratio of M2-like TAMs to TAMs = CD206 and CD68 colocalization fluorescence intensity / CD68 fluorescence intensity (n = 3) (P** < 0.01, P*** < 0.001).

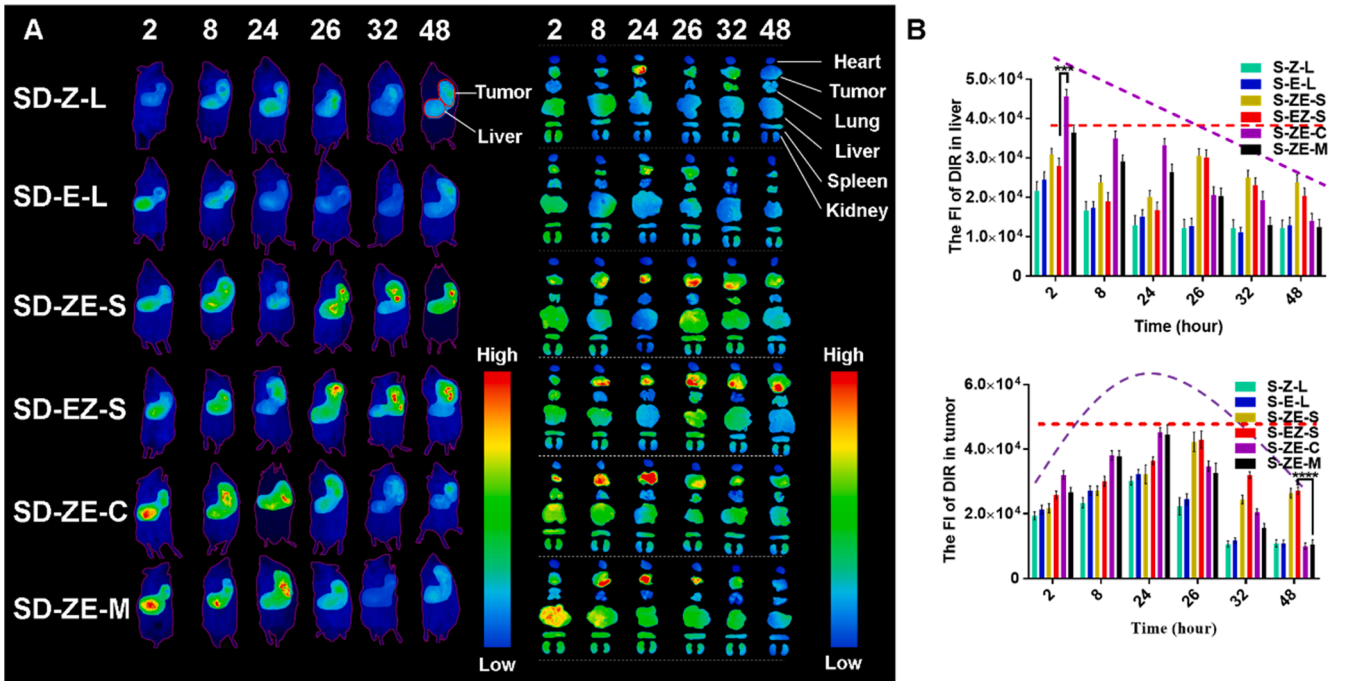

Fig. 6. *In vivo* liposome targeting by different combined administration methods. (A) *In vivo* cumulative fluorescence intensity of DIR at 2, 8, 24, 26, 32, and 48 h after injection of DIR-modified liposomes (n = 2). (B) Quantitative analysis of DIR changes in liver and tumor ($P^{***} < 0.001$, $P^{****} < 0.0001$).

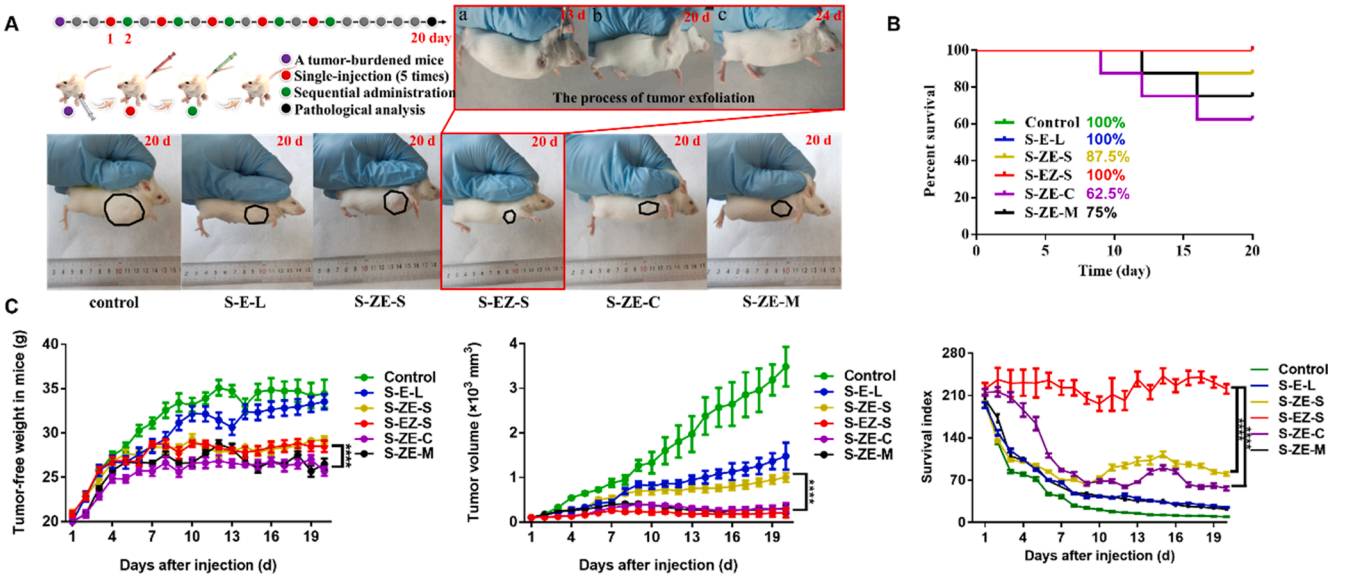

Fig. 7. (A) Schematic for pharmacodynamic monitoring in tumor-bearing mice treated for 20 days. (B) Survival analysis over 20 days in tumor-bearing mice. (C) Changes in the tumor volume, tumor-free weight, and Survival Index of tumor-bearing mice during treatment by different combined administration methods (n = 6 to 8). ($P^{****} < 0.0001$).

3.6. Pharmacodynamics and pathology of different combined administration methods

Differences in therapeutic and toxicity effects of combined administration methods were observed in a 20-day pharmacodynamics experiment. Tumor growth rates were significantly lower in the S-EZ-S than in the S-ZE-S treatment ($P < 0.001$). The S-EZ-S treatment showed no increase in tumor volume and 25% tumor shedding (Fig. 7A and C). Moreover, the number of tumor cells in the S-EZ-S treatment was significantly lower than that in the S-ZE-S and S-ZE-C treatments ($P < 0.001$; Fig. 8B and C), and apoptosis rates in the S-EZ-S treatment were significantly higher than those in treatment S-ZE-S ($P < 0.001$; Fig. 8C); however, tumor growth rates did not differ significantly between S-ZE-M and S-ZE-C treatments (Fig. 7C). In treatment with S-EZ-S, the increase in tumor-free weight was significantly higher than that in treatments with S-ZE-C and S-ZE-M ($P < 0.001$). Survival rates after treatment with S-EZ-S, after single administration of S-E-L, and the controls were 100%, and no indication of drug toxicity was observed in the heart, liver, lung, and kidney sections after treatment with S-EZ-S (Fig. 8A). The survival rates in treatments with S-ZE-S, S-ZE-M, and S-ZE-C were 87.5%, 75%, and 62.5%, respectively. Cardiomyocytes of S-ZE-M mice showed slight myocardial ruptures. Small extent of inflammatory cell infiltration in the

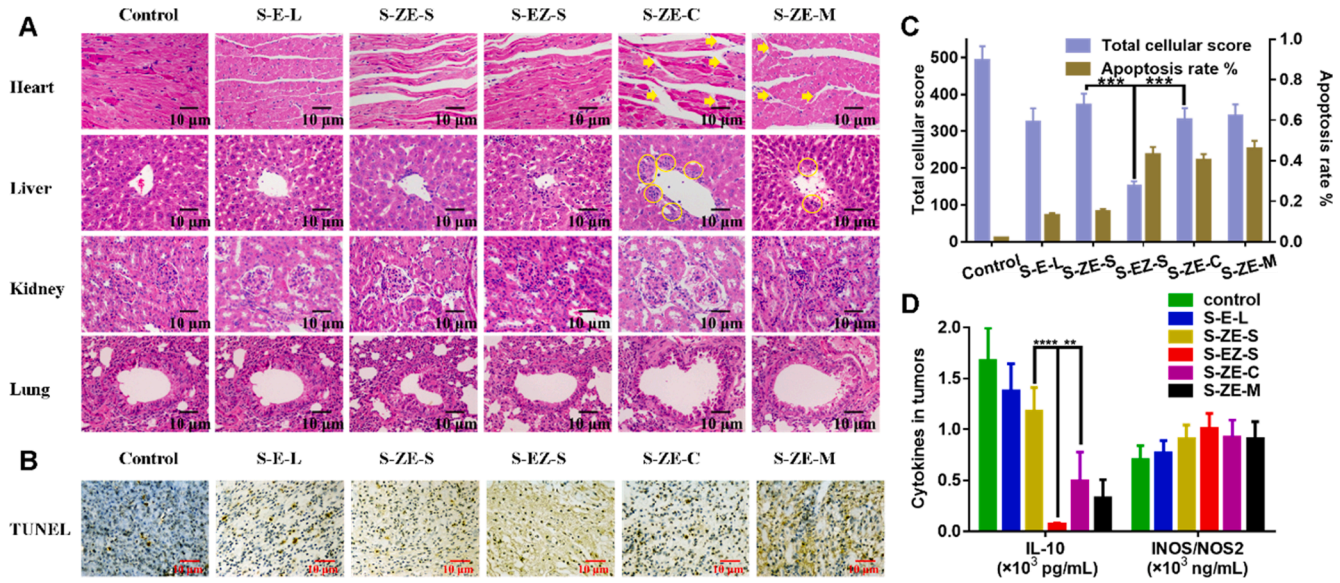

Fig. 8. (A) Histopathology of heart, liver, kidney, and lung sections from the different treatment groups; tissues were stained with hematoxylin and eosin (H&E). Yellow arrows indicate abnormal regions in the cardiomyocytes and liver. Scale bar: 10 μm. (B) TUNEL was used to measure the degree of apoptosis of tumor cells treated using different administration groups. Scale bar: 10 μm. (C) The rate of apoptosis calculated by ImageJ. (D) Changes of IL-10 and iNOS/NOS2 in tumors after treatment (n = 3) (P** < 0.01, P*** < 0.001, P**** < 0.0001).

hepatic portal vein, slightly dilated renal capsules, and slightly enlarged glomeruli were observed (Fig. 8A). The most severe damage was observed in treatment with S-ZE-C, showing severe myocardial ruptures, blurred edges of myocardial cell structures, and severe inflammatory cell infiltration. The structure of liver lobules was compromised, the structure of liver cells was incomplete, the boundaries were not clear, the arrangement was chaotic, and a large number of inflammatory cells had infiltrated the hepatic portal vein. The renal capsule was severely dilated and the glomeruli were enlarged. The SI of S-ZE-S was significantly higher than that of the other treatments ($P < 0.001$; Fig. 7C), demonstrating that treatment with S-EZ-S resulted in improved efficacy and reduced toxicity compared to other treatments.

4. Discussion

4.1. Molecular docking, synthesis, and characterization of SA-ODA

As deduced from the MS data, the main molecular ions were observed at 583.4 Da $[SA\text{-}ODA + Na]^+$ and 595.4 Da $[SA\text{-}ODA + Cl]^-$ (Fig. 1B). ^1H NMR (CD3OD, ppm) showed 0.8 (t, 3H, H-11), 1.19 (s, 30H, alkyl), 1.22 (m, 2H, H-2), 1.43 (m, 1H, H-3), 1.92 (s, 3H, H-10), 2.19 (m, 1H, H-30), 3.10 (t, 2H, H-1), 3.93 (d, 1H, H-7), 3.57 (m, 2H, H-90, H-8), 3.71 (m, 2H, H-9, H-5), and 3.91 (m, 2H, H-6, H-4). Regarding ODA, the characteristic peaks at 0.8, 1.43, and 3.10 remained, and the peaks of $–NH_2$ did not; the characteristic SA peaks at 1.19, 1.22, 1.92, 2.19, 3.93, 3.57, 3.71, and 3.91 remained, whereas those of –COOH did not (Zhennan She et al. 2014, Tang et al. 2020). Thus, SA-ODA was successfully synthesized and retained the ability to target Siglec-1.

4.2. Preparation and characterization of liposomes

Interaction with the primary amino group of EPI and the phosphonate group of ZOL may increase the probability of intermolecular contact in a mixed solution containing ZOL and EPI (ZE-S) through electrostatic attractions to form ionic and/or hydrogen bonds and low-solubility aggregates (Fig. 2A). When liposomes containing ZOL were loaded with EPI, the encapsulation rates of ZOL and EPI remained unchanged (Table 3). “Coffee-bean” particles were formed due to low-solubility of EPI and ZOL aggregates, EPI, and sulfate radicals. In *in vitro* release experiments, EPI formed low-solubility aggregates in S-E-L and S-ZE-L, and the release rate of EPI was unchanged; however, ZOL formed low-solubility aggregates in S-ZE-L. Thus, the release rate of ZOL was different.

4.3. Cytotoxicity and uptake in polarized RAW264.7 cells in vitro

The characteristics and structures of liposomes were the same; thus, the number of liposomes taken up by cells was assumed to be equal. In the S-EZ-S and S-ZE-S treatments, the number of nanoparticles taken up was the same after the first administration as that in the S-ZE-C, S-Z-L, and S-E-L treatments. This was likely due to only a portion of the cells taking up liposomes after the first administration, which limited the overall uptake. Regarding S-ZE-M, the number of nanoparticles exceeded the uptake capacity per time unit. In the S-ZE-C treatment, when the same number of liposomes was taken up by cells, intracellular accumulation of drugs increased because both drugs were encapsulated in each liposome. In the cytotoxicity experiment with the S-EZ-S treatment, killing of colony-forming TAMs and highly differentiated M2-like TAMs reduced cell densities and resulted in phenotype reversal of newly produced M2-like TAMs. Compared with S-ZE-S, S-EZ-S increased the effect of ZOL; however, in S-ZE-C with both EPI and ZOL taken up by each cell at the same time, the cytotoxic effect was stronger than the effect of phenotypic reversal; therefore, the effect of ZOL was obscured. Regarding S-ZE-M, the two types of liposomes were taken up randomly, causing inconsistency of therapeutic effects. In summary, for the different combined administration regimens of EPI and ZOL, owing to the different mechanisms of action of EPI and ZOL, there was a non-linear relationship between uptake by liposomes and cytotoxicity.

4.4. Phenotypic reversal of M2-like TAMs in vitro and in vivo

Our findings demonstrated that cytotoxic effects and phenotypic reversal differed between administration regimens. Phenotype reversal was indicated by decreased fluorescence intensity of CD206, reduced secretion of IL-10, and lower numbers of M2-like TAMs. Decrease in fluorescence intensity of CD68 and increase in fluorescence intensity of PI indicated lower total number of TAMs. iNOS/NOS2 secretion remained unchanged, indicating that the number of M1-like TAMs was

not affected. Moreover, the proportion of M2-like TAMs had decreased more than overall TAM numbers, suggesting that some M2-like TAMs had transformed into M1-like TAMs. Treatment with S-EZ-S showed better therapeutic effects than that with S-ZE-S, because treatment with the latter resulted in reduced cell densities, elimination of highly differentiated M2-like TAMs, and phenotype reversal of newly produced M2-like TAMs in tumors. In treatment with S-ZE-C, EPI and ZOL were taken up synchronously by the cells, which would imply that cytotoxic and phenotypic reversal effects occurred simultaneously; thus, the effect of ZOL was masked by that of EPI. In treatment with S-ZE-M, either one or both drugs were taken up by cells, causing erratic effects.

4.5. Compound distribution in tissues in vivo

Because of the focused targeting of TAMs by SA-modified liposomes, DIR did not accumulate in the heart, spleen, lungs, and kidneys. A significant difference in DIR accumulation occurred between liver and tumor tissue in the combined administration regime. In treatments with S-EZ-S and S-ZE-S, the number of particles in the liver was lower owing to reduced dosages administered with a single injection, and DIR accumulation within tumors was increased owing to higher numbers of injections. Regarding S-ZE-M, the ability of tumor cells to take up the compounds was limited because large numbers of liposomes were trapped in the liver. Regarding treatment with S-ZE-C, as DIR in a single liposome was double that of the other groups, DIR levels was increased in the liver after 2 h. When the number of particles and the amount of drug exceed the range of the targeting ability, the non-linearity of dose response and off-target damage increase (Chou 2010, Ottewell et al. 2010, (EBCTCG) (2019)).

4.6. Pharmacodynamics and pathology of different combined administration methods

In combined administration treatments, therapeutic effects and toxicity of different combined administration methods were closely associated with the mechanisms of action of EPI and ZOL and with their dosages. The SI suggested that the treatment effect of S-EZ-S was significantly stronger than that of the other treatments; however, there was no significant difference in the unilateral analysis of tumors, weight, survival ratio, and other parameters, suggesting limitations of this type of analysis. Therefore, even though tumor growth rates in the S-ZE-C and S-ZE-M treatments did not differ from those in the S-EZ-S treatment, deaths as well as severe pathological damage and weight loss were observed in mice in the S-ZE-C and S-ZE-M groups. S-EZ-S treatment showed no mortality and exhibited 25% tumor shedding due to separated administration of EPI and ZOL. Even though a certain therapeutic effect was observed, physiological damage was severe; the survival rates in the S-E-L, control, and S-EZ-S groups were 100%; however, tumor growth rates in the S-E-L and control groups were not effectively reduced. S-EZ-S effectively inhibited tumor growth with 100% survival and achieved 25% tumor shedding owing to sequential drug administration, which is not merely the cumulative effect of each of the two drugs, but results from a complementary mechanism of action of the two compounds: the first injection with S-E-L killed TAMs and reduced highly differentiated M2-like TAMs in proximity of the tumor, and subsequent administration of S-Z-L reversed the phenotype of newly produced M2-like TAMs, resulting in cytotoxicity. However, S-E-L and control treatments showed tumor-free weight reduction due to reduced dosages without producing other therapeutic effects (such as those offered by sequential administration due to presence of highly differentiated M2-like TAMs in the periphery and near high-density tumor cells), and the therapeutic effect of S-Z-L decreased.

4.7. Comprehensive analysis of different combined administration methods

Compared to S-ZE-C and S-ZE-M treatments, in treatment S-EZ-S, the single drug doses were reduced (injection of S-E-L or S-Z-L in batches), and the injections were more frequent; moreover, DIR was reduced in the liver after 2 h and drug accumulation in the liver and spleen was increased after 48 h (Fig. 6A, B). Following S-EZ-S treatment, the heart, liver, kidneys, and lungs showed no obvious damage, and the number of apoptotic tumor cell was significantly increased (Fig. 8A, B) with 100% survival (Fig. 7). Compared to S-ZE-S, S-EZ-S treatment significantly reduced the number of cells in tumors by killing highly differentiated M2-like TAMs and reducing cell densities and then reversing new M2-like TAMs. Tumor cell growth was effectively inhibited (Fig. 8B), and the number of reversed M2-like TAMs was increased.

5. Conclusions

Or results demonstrate that different methods of combined administration of EPI and ZOL exert different therapeutic effects. S-EZ-S treatment resulted in accumulation of the drugs in tumors to a great extent and low retention by the liver owing to reduced single-injection dosages and more frequent injections, which helped improve efficacy and reduce toxicity. Following S-EZ-S treatment, the effect of EPI on TAM colonies and highly differentiated M2-like TAMs was effectively combined with the effect of ZOL on phenotype reversal of M2-like TAMs to achieve a synergistic treatment effect. S-EZ-S treatment resulted in no tumor growth, no toxicity of noncancerous tissue, and no deaths of mice, with 25% tumor shedding. Taken together, in combined treatments targeting TAMs, treatment with S-EZ-S using SA-modified liposomes can improve the antitumor effects of EPI and ZOL.

CRediT authorship contribution statement

Dezhi Sui: Methodology, Investigation, Writing - original draft. **Xueying Tang:** Investigation, Writing - review & editing. **Junqiang Ding:** Investigation, Writing - review & editing. **Yang Wang:** Investigation. **Ying Qin:** Investigation, Writing - review & editing. **Ning Zhang:** Writing - review & editing. **Xinrong Liu:** Writing - review & editing. **Yihui Deng:** Writing - review & editing. **Yanzhi Song:** Conceptualization, Writing - review & editing, Project administration.

Declaration of Competing Interest

The authors declare that they have no known competing financial interests or personal relationships that could have appeared to influence the work reported in this paper.

Acknowledgments

This study was supported by the National Natural Science Foundation of China (grant number 81703456).

References

(EBCTCG), E. B. C. T. C. G., 2019. Increasing the dose intensity of chemotherapy by more frequent administration or sequential scheduling: a patient-level meta-analysis of 37 298 women with early breast cancer in 26 randomised trials. The Lancet, 393, 1440–1452.

Aryal, S., Hu, C.-M.-J., Zhang, L., 2011. Polymeric Nanoparticles with Precise Ratiometric Control over Drug Loading for Combination Therapy. Mol. Pharmaceutics 8, 1401–1407.

Benyettou, F., Alhashimi, M., O'Connor, M., Pasricha, R., Brandel, J., Traboulsi, H., Mazher, J., Olsen, J.-C., Trabolsi, A., 2017. Sequential Delivery of Doxorubicin and Zoledronic Acid to Breast Cancer Cells by CB[7]-Modified Iron Oxide Nanoparticles. ACS Appl. Mater. Interfaces 9 (46), 40006–40016.

Cao, Y., Roursgaard, M., Jacobsen, N.R., Moller, P., Loft, S., 2016. Monocyte adhesion induced by multi-walled carbon nanotubes and palmitic acid in endothelial cells and alveolar-endothelial co-cultures. Nanotoxicology 10, 235–244.

Chou, T.-C., 2010. Drug combination studies and their synergy quantification using the Chou-Talalay method. Cancer Res. 70 (2), 440–446.
Cui, JingXia, Li, ChunLei, Guo, WenMin, Li, YanHui, Wang, CaiXia, Zhang, L.i., Zhang, L., Hao, YanLi, Wang, YongLi, 2007. Direct comparison of two pegylated liposomal doxorubicin formulations: is AUC predictive for toxicity and efficacy? J. Control Release 118 (2), 204–215.
Ding, J., Zhao, D., Hu, Y., Liu, M., Liao, X., Zhao, B., Liu, X., Deng, Y., Song, Y., 2019. Terminating the renewal of tumor-associated macrophages: A sialic acid-based targeted delivery strategy for cancer immunotherapy. Int. J. Pharm. 571, 118706. https://doi.org/10.1016/j.ijpharm.2019.118706.
Eisenblatter, M., Ehrchen, J., Varga, G., Sunderkotter, C., Heindel, W., Roth, J., Bremer, C., Wall, A., 2009. In vivo optical imaging of cellular inflammatory response in granuloma formation using fluorescence-labeled macrophages. J. Nucl. Med. 50 (10), 1676–1682.
Giarra, S., Zappavigna, S., Campani, V., Abate, M., Cossu, A., Leonetti, C., Porru, M., Mayol, L., Caraglia, M., De Rosa, G., 2018. Chitosan-Based Polyelectrolyte Complexes for Doxorubicin and Zoledronic Acid Combined Therapy to Overcome Multidrug Resistance. Pharmaceutics 10 (4), 180. https://doi.org/10.3390/pharmaceutics10040180.
Haran, G., Cohen, R., Bar, L.K., Barenholz, Y., 1993. Transmembrane ammonium sulfate gradients in liposomes produce efficient and stable entrapment of amphipathic weak bases.pdf. Biochimica et Biophysica Acta 1151 (2), 201–215.
Hu, Q., Sun, W., Wang, C., Gu, Z., 2016. Recent advances of cocktail chemotherapy by combination drug delivery systems. Adv. Drug Deliv. Rev. 98, 19–34.
Kopecka, J. P., S.; Lusa, S (2016) Zoledronic acid-encapsulating self-assembling nanoparticles and doxorubicin: a combinatorial approach to overcome simultaneously chemoresistance and immunoresistance in breast tumors. Oncotarget, 7, 20753–20772.
Liu, C., Li, C., Pang, C., Li, M., Li, H., Li, P., Fan, L.i., Liu, H., Tian, W., 2020. Supramolecular Drug-Drug Complex Vesicles Enable Sequential Drug Release for Enhanced Combination Therapy. ACS Appl. Mater. Interfaces 12 (25), 27940–27950.
Liu, M., Luo, X., Qiu, Q., Kang, L., Li, T., Ding, J., Xiong, Y., Zhao, Z., Zan, J., Chang, C., Liu, X., Song, Y., Deng, Y., 2018. Redox- and pH-Sensitive Glycan (Polysialic Acid) Derivatives and F127 Mixed Micelles for Tumor-Targeted Drug Delivery. Mol. Pharmaceutics 15, 5534–5545.
Ma, Y., Adjemian, S., Mattarollo, S., Yamazaki, T., Aymeric, L., Yang, H., Portela Catani, J., Hannani, D., Duret, H., Steegh, K., Martins, I., Schlemmer, F., Michaud, M., Kepp, O., Sukkurwala, A., Menger, L., Vacchelli, E., Droin, N., Galluzzi, L., Krzysiek, R., Gordon, S., Taylor, P., Van Endert, P., Solary, E., Smyth, M., Zitvogel, L., Kroemer, G., 2013. Anticancer chemotherapy-induced intratumoral recruitment and differentiation of antigen-presenting cells. Immunity 38 (4), 729–741.
Makwana, V., Karanjia, J., Haselhorst, T., Anoopkumar-Dukie, S., Rudrawar, S., 2021. Liposomal doxorubicin as targeted delivery platform: Current trends in surface functionalization. Int. J. Pharmaceut. 593.
Miquel Pons, M.F., Joan Estelrich, 1993. Liposomes obtained by the ethanol injection method. Int. J. Pharmaceut., 51–56.
Ottewell, P.D., Lefley, D.V., Cross, S.S., Evans, C.A., Coleman, R.E., Holen, I., 2010. Sustained inhibition of tumor growth and prolonged survival following sequential administration of doxorubicin and zoledronic acid in a breast cancer model. Int. J. Cancer 126 (2), 522–532.
Ovais, M., Guo, M., Chen, C., 2019. Tailoring Nanomaterials for Targeting Tumor-Associated Macrophages. Adv. Mater. 31 (19), 1808303.
Allavena, P., Mantovani, A., 2012. Immunology in the clinic review series; focus on cancer: tumour-associated macrophages: undisputed stars of the inflammatory tumour microenvironment. Clin. Exper. Immunol. 167, 195–205.
R.H.Müller, S.R., 1993. In vitro phagocytosis assay of nano- and microparticles bychemiluminescence. III. Uptake of differently sized surface-modifiedparticles, and its correlation to particle properties and in vivodistribution. Eur. J. Pharmaceut. Sci., 1, 31–39.
Rodell, C.B., Arlauckas, S.P., Cuccarese, M.F., Garris, C.S., Li, R., Ahmed, M.S., Kohler, R. H., Pittet, M.J., Weissleder, R., 2018. TLR7/8-agonist-loaded nanoparticles promote the polarization of tumour-associated macrophages to enhance cancer immunotherapy. Nat. Biomed. Eng. 2 (8), 578–588.
Sun, R., Liu, Y., Li, S.-Y., Shen, S., Du, X.-J., Xu, C.-F., Cao, Z.-T., Bao, Y., Zhu, Y.-H., Li, Y.-P., Yang, X.-Z., Wang, J., 2015. Co-delivery of all-trans-retinoic acid and doxorubicin for cancer therapy with synergistic inhibition of cancer stem cells. Biomaterials 37, 405–414.
Tang, X., Sui, D., Liu, M., Zhang, H., Liu, M., Wang, S., Zhao, D., Sun, W., Liu, M., Luo, X., Lai, X., Liu, X., Deng, Y., Song, Y., 2020. Targeted delivery of zoledronic acid through the sialic acid - Siglec axis for killing and reversal of M2 phenotypic tumor-associated macrophages – A promising cancer immunotherapy. Int. J. Pharmaceut. 590, 119929. https://doi.org/10.1016/j.ijpharm.2020.119929.
Vinciguerra, D., Jacobs, M., Denis, S., Mougin, J., Guillaneuf, Y., Lazzari, G., Zhu, C., Mura, S., Couvreur, P., Nicolas, J., 2019. Heterotelechelic polymer prodrug nanoparticles: Adaptability to different drug combinations and influence of the dual functionalization on the cytotoxicity. J. Control Release 295, 223–236.
Weber, J.S., Gibney, G., Sullivan, R.J., Sosman, J.A., Slingluff, C.L., Lawrence, D.P., Logan, T.F., Schuchter, L.M., Nair, S., Fecher, L., Buchbinder, E.I., Berghorn, E., Ruisi, M., Kong, G., Jiang, J., Horak, C., Hodi, F.S., 2016. Sequential administration of nivolumab and ipilimumab with a planned switch in patients with advanced melanoma (CheckMate 064): an open-label, randomised, phase 2 trial. Lancet Oncol. 17 (7), 943–955.
Wei, X., Wang, Y.i., Xiong, X., Guo, X., Zhang, L., Zhang, X., Zhou, S., 2016a. Codelivery of a π-π Stacked Dual Anticancer Drug Combination with Nanocarriers for Overcoming Multidrug Resistance and Tumor Metastasis. Adv. Funct. Mater. 26 (45), 8266–8280.
Wei, X.-F., Shimizu, Y., Kanai, M., 2016b. An Expeditious Synthesis of Sialic Acid Derivatives by Copper(I)-Catalyzed Stereodivergent Propargylation of Unprotected Aldoses. ACS Cent. Sci. 2 (1), 21–26.
Wu, D., Pusuluri, A., Vogus, D., Krishnan, V., Shields, C.W., Kim, J., Razmi, A., Mitragotri, S., 2020. Design principles of drug combinations for chemotherapy. J Control Release 323, 36–46.
Xia, Y., Xie Y., Yu, Z., 2018. The Mevalonate Pathway Is a Druggable Target for Vaccine Adjuvant Discovery. Cell, 175, 1059–1073.
Yang, Q., Xiao, Y., Yin, Y., Li, G., Peng, J., 2019. Erythrocyte Membrane-Camouflaged IR780 and DTX Coloading Polymeric Nanoparticles for Imaging-Guided Cancer Photo-Chemo Combination Therapy. Mol. Pharmaceutics 16, 3208–3220.
Zhang, T., She, Z., Huang, Z., Li, J., Luo, X., Deng, Y., 2014. Application of sialic acid/polysialic acid in the drug delivery systems. Asian J. Pharmaceut. Sci. 9 (2), 75–81.
Zheng, H., Li, J., Wang, M., Luo, X., Qiu, Q., Hu, L., LI, C., Song, Y., Deng, Y., 2019. Exhausting tumor associated macrophages with sialic acid-polyethyleneimine-cholesterol modified liposomal doxorubicin for enhancing sarcoma chemotherapy. Int. J. Pharm. 558, 187–200.
She, Z., Zhang, T., Wang, X., Li, X., Song, Y., Cheng, X., Huang, Z., Deng, Y., 2014. The anticancer efficacy of pixantrone-loaded liposomes decorated with sialic acideoctadecylamine conjugate. Biomaterials 35, 5216–5225.